

# Anomaly Detection with Deep Perceptual Autoencoders

Nina Tuluptceva<sup>1,2</sup>[0000-0003-0910-188X], Bart Bakker<sup>1</sup>[0000-0002-1438-8136],  
Irina Fedulova<sup>1</sup>[0000-0002-5959-5382], Heinrich Schulz<sup>1</sup>[0000-0003-4048-2254], and  
Dmitry V. Dylov<sup>2</sup>[0000-0003-2251-3221]

<sup>1</sup> Philips Research

nina.tuluptceva, bart.bakker@philips.com  
irina.fedulova, heinrich.schulz@philips.com

<sup>2</sup> Skolkovo Institute of Science and Technology  
d.dylov@skoltech.ru

**Abstract.** Anomaly detection is the problem of recognizing abnormal inputs based on the seen examples of normal data. Despite recent advances of deep learning in recognizing image anomalies, these methods still prove incapable of handling complex medical images, such as barely visible abnormalities in chest X-rays and metastases in lymph nodes. To address this problem, we introduce a new powerful method of image anomaly detection. It relies on the classical autoencoder approach with a re-designed training pipeline to handle high-resolution, complex images and a robust way of computing an image abnormality score. We revisit the very problem statement of fully unsupervised anomaly detection, where no abnormal examples at all are provided during the model setup. We propose to relax this unrealistic assumption by using a very small number of anomalies of confined variability merely to initiate the search of hyperparameters of the model. We evaluate our solution on natural image datasets with a known benchmark, as well as on two medical datasets containing radiology and digital pathology images. The proposed approach suggests a new strong baseline for image anomaly detection and outperforms state-of-the-art approaches in complex medical image analysis tasks.

**Keywords:** Anomaly Detection · Autoencoders · Chest X-Rays · Radiology · Digital Pathology

## 1 Introduction

Anomaly detection is a crucial task in the deployment of machine learning models, where knowing the “normal” data samples should help spot the “abnormal” ones [4, 6]. If an input deviates from the training data substantially, it is usually impossible to predict how the model will behave [2, 20]. This makes it essential for high-consequence applications, such as medical decision support systems, to know how to recognize the anomalous data. Identification of rare occurrences is another important application where anomaly detection is useful. For example,

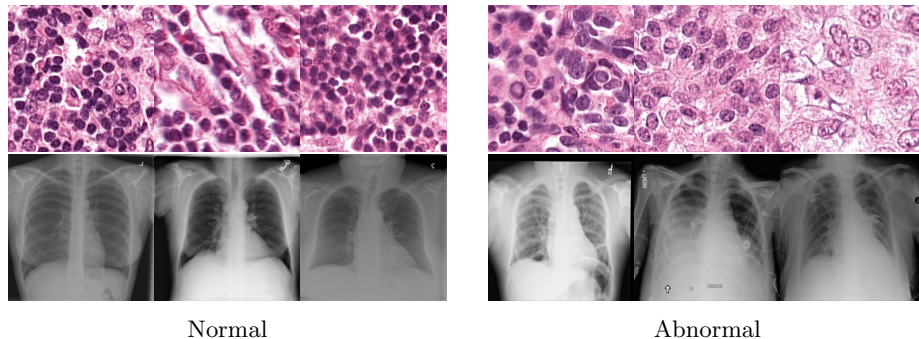


Fig. 1: Examples of normal vs abnormal images of H&E-stained lymph node of Camelyon16 challenge [3] (top) and chest X-rays of NIH dataset [29] (bottom).

in pathology, where labeling diverse microscopy datasets is both time-consuming and expensive, the rare types of cells and tissues require specialized expertise from the annotator [8, 17]. Because the normal cases greatly prevail over the abnormal one, anomaly detection algorithms can largely alleviate the annotation burden and automatically point to the rare samples.

In recent years, deep learning techniques achieved important advances in image anomaly detection [10, 11, 21–23, 25, 27, 30]. However, these efforts were primarily focused on artificial problems with distinct anomalies in natural images (e.g., outliers in images of “cats” in the CIFAR10 dataset [18]). The medical anomalies, however, differ from those in the natural images [21, 25, 26]. The medical image anomalies tend to resemble the normal data much more strongly, being much “closer” to them by the distribution. For example, detection of obscure neoplasms in chest X-rays [29] and of metastases in H&E-stained lymph node images [3] manifest a blatant challenge at hand, with the anomalous tissues being barely different from the normal ones (Figure 1).

In our paper, we evaluate and compare existing state-of-the-art (SOTA) approaches ([25], [27] and [21]) on the two aforementioned medical tasks. We find these methods either to struggle detecting such types of abnormalities, or to require a lot of time and resources for training. Besides, the SOTA approaches lack a robust way of setting up model hyperparameters on new datasets, which complicates their use. Thus, we revisit the problem of image anomaly detection and introduce a new powerful approach, capable of tackling these challenges in the medical domain. The proposed method leverages the efficacy of *autoencoders* for anomaly detection [13], the expressiveness of *perceptual loss* [15] for understanding the content in the images, and the power of the *progressive growth* [16] to handle training on high-dimensional image data.

Recent related studies showed the effectiveness of deep features as a perceptual metric between images (perceptual loss), and as a score of anomaly [9, 15, 27, 31]. Also, the use of the perceptual loss for training autoencoders has been very popular in a variety of tasks [5, 14, 15, 27, 31] except for the task of anomaly de-

tection which has been inexplicably somewhat dismissed so far. Trained only on normal data, autoencoders tend to produce a high reconstruction error between the input and the output when the input is an abnormal sample. That property has been used intensively for anomaly detection [1, 7, 11, 22, 30, 32]. We propose to compel the autoencoder to reconstruct *perceptive* or *content* information of the normal images, by using *only* the perceptual loss during autoencoder training. As such, the reconstructed image may not be an image altogether, but a tensor that stores the “content” of the input image. The main idea behind it is not to force the network to reconstruct a realistic looking image, but to let it be flexible in understanding the content of the normal data. Section 2.1 covers the details.

To further improve the expressiveness of the autoencoder and to allow it to capture even the fine details in the data, we propose to train the model using progressive growing technique [12, 16], starting from a low-resolution network and adding new layers to gradually introduce additional details during the training. In particular, we present how to achieve a smooth growth of perceptual information in the loss function, and show that this improves the quality of anomaly detection in the high-resolution medical data. We will describe it in Section 2.2.

Lastly, we propose a new approach to the basic setup of anomaly detection model. Most approaches [10, 22, 23, 27, 30] prescribe not to use any anomaly examples during the model setup, dismissing the questions of optimization and of hyperparameter selection for such models. However, in reality, some types of abnormalities to detect are actually known (for example, the most frequent pathologies on the chest X-rays). Therefore, we consider the *weakly-supervised* scenario where a low number of anomalies with confined variability are available for use in optimal model hyperparameter selection (Section 2.3). We believe this scenario reflects the real tasks encountered in practice, provides a clear pipeline for setting up the model on new data, and helps to obtain reproducible results.

To summarize our main results quantitatively, the proposed solution achieves 0.934 ROC AUC in the detection of metastases in H&E stained images of lymph nodes (Camelyon16 dataset [3]), and 0.926 in the detection of abnormal chest X-rays (subset of NIH dataset [29]). This outperforms SOTA methods.

## 2 Method

### 2.1 Deep Perceptual Autoencoder

Autoencoder-based approaches rely on the fact that autoencoders can learn shared patterns of the normal images and, then, restore them correctly. The key idea of our method is to simplify the learning of these common factors inherent to the data, by providing a loss function that measures “pattern”-dissimilarity of the input and the output. It was shown that the perceptual loss – which computes a distance between the deep features obtained from an object classification neural network pre-trained on a large diverse dataset – can capture the “content” dissimilarity of the images [9, 15]. We further propose to use *only* the perceptual loss to train the autoencoder and to compute the restoration error during the

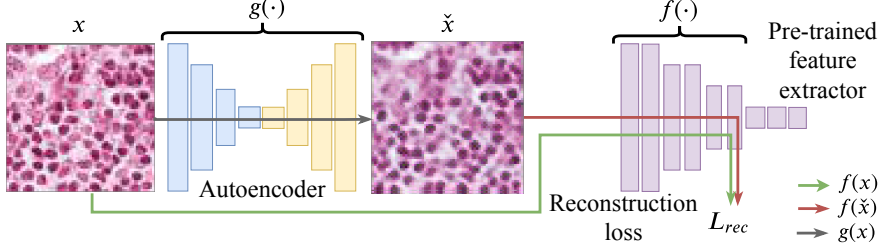


Fig. 2: The proposed Deep Perceptual Autoencoder for image anomaly detection.

evaluation, without considering the loss term that compels to restore the whole input information in an image. We will show that such a loss allows the autoencoder more flexibility to gain a meaningful understanding of the “normality” of the data, leading to much better results.

Figure 2 illustrates our approach, which we called Deep Perceptual Autoencoder. Let  $g$  be the autoencoder network, and  $x$  be an image. During the training, the autoencoder minimizes the difference between  $x$  and the reconstructed “image”  $\tilde{x} = g(x)$ , being called the reconstruction loss  $L_{rec}(x, \tilde{x})$ . To compute the perceptual loss as the reconstruction loss between  $x$  and  $\tilde{x}$ , we compute the difference between the deep features of these images ( $f(x)$  and  $f(\tilde{x})$ , respectively). We adopt relative-perceptual-L1 loss from Ref. [27] as it is robust to noise and to the changes in the image contrast perceptual metric:  $L_{rec}(x, \tilde{x}) = \frac{\|\hat{f}(x) - \hat{f}(\tilde{x})\|_1}{\|\hat{f}(x)\|_1}$ , where  $\hat{f}(x) = \frac{f(x) - \mu}{\sigma}$  are the normalized features with pre-calculated on a large dataset the mean  $\mu$  and the standard deviation  $\sigma$  of the filter responses of the layer. In the evaluation stage, the same  $L_{rec}(x, g(x))$  is used to predict the abnormality in the new input  $x$ .

## 2.2 Progressive Growing

In order to improve the expressive power of the autoencoder in Figure 2, we propose to train it by harnessing the power of progressive growth [16]. Illustrated in Figure 3, the suggested pipeline gradually *grows* the “level” of the “perceptual” information in the loss function. In the beginning of the training, the loss function computes the dissimilarity between the low-resolution images using the features from the coarse layers of the network, whereas, as the training advances, the “level” of this information is increased by including deeper and deeper features. It seems intuitively essential because the “content” information is absent in the low-resolution images, with only the main color and the high-level structure being stored there. The novelty that we propose in our solution, therefore, is to *synchronize* addition of the new layers to the autoencoder with the gradual increase of the depth of the features entailed in the calculation of the perceptual loss (see Figure 3(Right) below).

Both the autoencoder  $g$  and the perceptual loss  $L_{rec}$  have a low “resolution” in the beginning (Figure 3(Left)). For example, the input and the output of

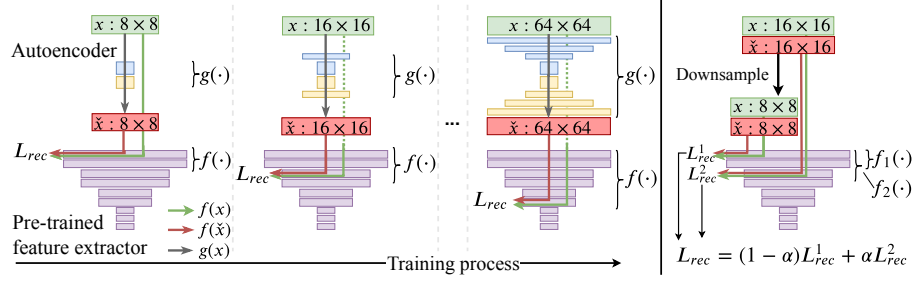


Fig. 3: Progressive training process. (Left) The layers are incrementally faded to the autoencoder  $g$ , and the depth of the features  $f$  increases synchronously. (Right) The gradual increase of the “resolution” of the perceptual loss  $L_{rec}$ .

the autoencoder are  $8 \times 8$ -pixel images  $x$  and  $\tilde{x}$ , and the loss  $L_{rec}$  computes the distance between the features  $f(x)$  and  $f(\tilde{x})$  of the coarse layer  $f$  (the pre-trained feature extractor network). As the training advances, the layers are incrementally added to the autoencoder  $g$ , and the depth of the features  $f$  is increased.

While doubling the resolution of the autoencoder, for example, from  $8 \times 8$  to  $16 \times 16$ , the new layers are introduced smoothly, with the parameter  $\alpha$  linearly increasing from 0 to 1 [12, 16]. As it was proposed in [12, 16], during this process, both the input  $x$  and the output  $\tilde{x}$  are the mixtures of the new high-resolution  $16 \times 16$  image and the previous low-resolution  $8 \times 8$  image, upsampled by a factor of two (not shown in Figure). In a similar manner, we smoothly increase the “level” of information supplied to  $L_{rec}$  from the features  $f_1$  to the features  $f_2$ :  $L_{rec} = \alpha * L_{rec}(f_2(x), f_2(\tilde{x})) + (1 - \alpha) * L_{rec}(f_1(\text{down}(x)), f_1(\text{down}(\tilde{x})))$ , where  $\text{down}(\cdot)$  carries out the downsampling by a factor of two.

### 2.3 Hyperparameters Tuning

Any anomaly detection model has many hyperparameters, the tuning of which is essential for the quality of the detection (in our method, these are the number of convolutions in the autoencoder, the size of the bottleneck, etc.). The majority of the anomaly detection papers declare no need to see the abnormal examples to set up their models, remaining vague with regard to how to choose the hyperparameters and how to deal with those cases when some new data needs to be analyzed by the same model. Some works mention tuning hyperparameters based on an unsupervised metric, like the value of the restoration error in the reconstruction-based methods [21, 22]. However, lower reconstruction loss does not mean better anomaly detection quality. For example, better reconstruction due to a larger bottleneck can cause the autoencoder to reconstruct anomalous data accurately as well.

In practice, however, one can have access to some labeled anomalies during the model setup. The number of such examples may be small, and they may not represent all possible abnormalities in the data, so it is typically tricky to use

them in training. In our work, we formulate a new *weakly-supervised* training scenario where a low number of labeled anomalous examples of a limited variation (i.e., a confined number of the types of anomalies) is available during the model setup as a “validation” or an “optimization” set. This small set serves a single purpose – select the model’s hyperparameters during its setup. Unlike works [21,26] that use a small subset of *all* anomalous data to improve the performance, we propose to use a small subset of *limited* types of anomalies merely for the initiation. This is a key difference because, in practice, it is difficult to cover all types of anomalies, even with just several examples of each. We believe that the proposed setting reflects real-world scenarios, allows consistent structuring of the experiments, and enables the generation of reproducible results.

### 3 Experiments

We evaluate approaches in the problem statement of a novelty detection, where the training data are assumed to be free of anomalies.

**Datasets and Evaluation Protocol.** We examine the detection of metastases in H&E stained images of lymph nodes in the Camelyon16 challenge [3] and the recognition of fourteen diseases on the chest X-rays in the NIH dataset [29] (Figure 1). We also evaluate the methods on two natural image benchmarks CIFAR10 [18] and SVHN [19] (the results are given in the supplementary material).

For all datasets, we use the published train-test sets. For the Camelyon16, we sampled the Vahadane-normalized [28]  $64 \times 64$  tiles from the fully “normal” slides with magnification of  $10\times$ , and treated these as “normal” (during the hyperparameter search, we also allowed the high-resolution images of the same patches with the magnification of  $20\times$  and  $40\times$ ). Tiles with metastases were treated as “abnormal”. NIH images without any disease marker were considered “normal”. We also separately examined the images with posteroanterior (PA) and anteroposterior (AP) projections and evaluated the models on a subset containing “clearer” normal/abnormal cases [26]. Default preprocessing of chest X-rays involved a  $768 \times 768$  central crop and resize to  $64 \times 64$ . During hyperparameter selection, we also considered resizing to  $128 \times 128$  (with and without the central crop) and histogram equalization. CIFAR10 and SVHN images were analyzed in a one-vs-all setting: one class of the dataset was considered as “normal” and all the others were treated as “abnormal”.

**Baselines.** We consider the following SOTA baselines: Deep GEO [10] (which uses the quality of classification of different geometric transformations of the image as an anomaly score), Deep IF [21] (extracts deep feature representations and feeds them into the isolation forest), and PIAD [27] (creates a mapping from the image distribution to the latent distribution by leveraging two GANs). We also compare our results on the NIH dataset to the GANs-based DAOL framework [26], purposely developed for detecting anomalies in chest X-rays.

Performance on CIFAR10 [18] and SVHN [19] we additionally compared with AnoGAN [25], GANomaly [1], DSEBM [30], and DeepSVDD [23] approaches (the results are provided in the supplementary material).

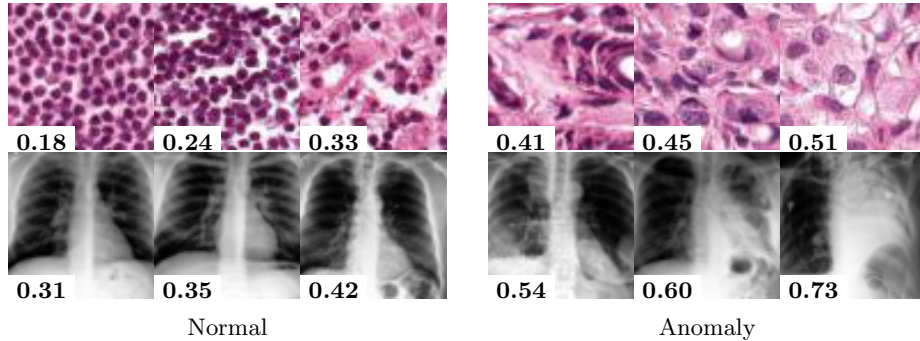


Fig. 4: Examples of normal and anomaly images with the predicted anomaly score. The higher the score, the more likely to be an anomaly. Datasets: Camelyon16 (top) and NIH subset (bottom).

**Implementation details.** We use autoencoders with residual blocks in all experiments. Hyperparameters are chosen by maximizing ROC AUC in a 3-fold cross-validation. For CIFAR10 and SVHN, we randomly sampled one abnormal class as a validation set, and for Camelyon16, we sampled images from 6 slides with metastases ( $\sim 5\%$  of all train examples). For validation on the NIH dataset, we used the most frequent disease (‘Infiltration’) out of fourteen possibilities. These conditions were fixed for all methods compared beneath.

The chosen hyperparameters reflect not only the model’s architecture and the training specifics (number of epochs, number of feature layers, depth of convolutions, etc.) but also the details of data preprocessing.

### 3.1 Results

For a legitimate comparison, we evaluate the baseline results both with the authors’ default model hyperparameters and with “the best” hyperparameters found by our cross-validation split (Table 1). Remarkably, our approach significantly outperforms Deep GEO and Deep IF in both medical datasets. The Deep GEO approach that uses geometric transformations to create a self-labeled dataset, shows poor performance on the digital pathology data, where the images are invariant to such transformations. Deep IF, which leverages a network pre-trained on ImageNet [24] to extract a compact data representation, recedes on the NIH dataset likely due to a large shift of the domain. Albeit with a smaller margin, we are also ahead of the PIAD method. In contrast to these 4-network architectures, though, our method uses only encoder and decoder, allowing a much simpler model setup (no need to search for a schedule of the adversarial training) and demanding less computational resources (training takes two networks instead of four and goes faster without the need for discriminators).

We illustrate the predictions of our model in Figure 4.

Table 1: ROC AUC in % with standard deviation (over 3 runs). For baselines we show results with their default hyperparameters and cross-validated. Bold font indicates the top score, italics – the second best.

	hyperparameters	Cam.16	NIH (a sub.)	NIH (PA)	NIH (AP)
DAOL	weakly-supervised	-	$80.5 \pm 2.1$	-	-
Deep GEO	default	$52.4 \pm 11.1$	$85.8 \pm 0.6$	$60.2 \pm 2.6$	$53.1 \pm 0.3$
	weakly-supervised	$45.9 \pm 2.1$	$85.3 \pm 1.0$	$63.6 \pm 0.6$	$54.4 \pm 0.6$
PIAD	default	$85.4 \pm 2.0$	<i><math>88.0 \pm 1.1</math></i>	$68.0 \pm 0.2$	$57.4 \pm 0.4$
	weakly-supervised	$89.5 \pm 0.6$	$87.3 \pm 0.9$	<i><math>68.7 \pm 0.5</math></i>	<b><math>58.6 \pm 0.3</math></b>
Deep IF	default	$87.6 \pm 1.5$	$76.6 \pm 2.7$	$52.2 \pm 0.5$	$54.3 \pm 0.5$
	weakly-supervised	<i><math>90.6 \pm 0.3</math></i>	$85.3 \pm 0.4$	$47.2 \pm 0.4$	$56.1 \pm 0.2$
Ours	weakly-supervised	<b><math>93.4 \pm 0.3</math></b>	<b><math>92.6 \pm 0.2</math></b>	<b><math>70.8 \pm 0.1</math></b>	$58.5 \pm 0.0$

### 3.2 Ablation study

To stress the importance of every component proposed herein, we performed an extensive ablation study. Table 2 considers six ablation scenarios.

**(1):** Autoencoder (AE) training with the perceptual loss (PL) and the hyperparameter optimization using *unsupervised* criteria (the reconstruction loss).

**(2):** The same, but with the hyperparameters corresponding to the best validation ROC AUC (*weakly-supervised* scenario).

**(3), (4) and (5):** Here, we added the adversarial loss (with weights 0.1 and 0.01) or L1 norm (with weight 1) to the loss function during the training (to force the reconstructed image to have a realistic look or to restore the whole input image).

**(6):** The last training scenario finally considers the progressive growing.

We observe that the method of selecting the hyperparameters by revealing a subset of anomalies of confined variability **(2)**, benefits the anomaly detection performance (compared to the unsupervised criteria **(1)**). The proposed progressive growing technique **(6)** also improves performance almost in all cases. We also note the advantage of our approach compared to the autoencoder, which encourages fully restored or realistic looking images **(3)-(5)** (using additional adversarial or L1 norm loss).

## 4 Conclusion

In this paper, we evaluated a range of state-of-the-art image anomaly detection methods, the performance of which we found to be sub-optimal in the challenging medical problems. We proposed a new method that uses an autoencoder to understand normal data representation, with optimization being performed with regard to perceptual loss in the regime of progressive growing training.



Table 2: Ablation study. ROC AUC in % with standard deviation (over 3 runs).

	Cam.16	NIH (a sub.)	NIH (PA)	NIH (AP)
(1) AE + PL (unsupervised)	87.9 $\pm$ 0.6	89.3 $\pm$ 0.2	68.9 $\pm$ 0.1	56.4 $\pm$ 0.2
(2) + weakly-supervised	92.7 $\pm$ 0.4	92.0 $\pm$ 0.2	70.3 $\pm$ 0.2	<b>58.6 <math>\pm</math> 0.1</b>
(3) + weakly-supervised + 0.1·adv	90.8 $\pm$ 0.7	82.2 $\pm$ 2.6	59.2 $\pm$ 1.4	55.4 $\pm$ 0.9
(4) + weakly-supervised + 0.01·adv	93.1 $\pm$ 0.6	90.8 $\pm$ 0.2	69.6 $\pm$ 0.6	58.6 $\pm$ 0.1
(5) + weakly-supervised + 1·L1	75.3 $\pm$ 1.6	91.7 $\pm$ 0.4	70.7 $\pm$ 0.2	57.3 $\pm$ 0.1
(6) + weakly-supervised + pr.gr	<b>93.4 <math>\pm</math> 0.3</b>	<b>92.6 <math>\pm</math> 0.2</b>	<b>70.8 <math>\pm</math> 0.1</b>	58.5 $\pm$ 0.0

To overcome the problem of setting up the model on new data, we propose to use a small set of anomalous examples of a limited variation – just to select the models hyperparameters. We believe that this realization reflects real-world scenarios, allowing consistent structuring of the experiments, and enabling the generation of reproducible results in the future. The proposed approach achieved 0.934 ROC AUC in the detection of metastases and 0.926 in the detection of abnormal chest X-rays. Our work establishes a new strong baseline for image anomaly detection.

## References

1. Akcay, S., Atapour-Abarghouei, A., Breckon, T.P.: Ganomaly: Semi-supervised anomaly detection via adversarial training. In: Asian conference on computer vision. pp. 622–637. Springer (2018)
2. Amodei, D., Olah, C., Steinhardt, J., Christiano, P., Schulman, J., Mané, D.: Concrete problems in ai safety. arXiv preprint arXiv:1606.06565 (2016)
3. Bejnordi, B.E., Veta, M., Van Diest, P.J., Van Ginneken, B., Karssemeijer, N., Litjens, G., Van Der Laak, J.A., Hermesen, M., Manson, Q.F., Balkenhol, M., et al.: Diagnostic assessment of deep learning algorithms for detection of lymph node metastases in women with breast cancer. *Jama* **318**(22), 2199–2210 (2017)
4. Chalapathy, R., Chawla, S.: Deep learning for anomaly detection: A survey. arXiv preprint arXiv:1901.03407 (2019)
5. Chan, C., Ginosar, S., Zhou, T., Efros, A.A.: Everybody dance now. In: Proceedings of the IEEE International Conference on Computer Vision. pp. 5933–5942 (2019)
6. Chandola, V., Banerjee, A., Kumar, V.: Anomaly detection: A survey. *ACM computing surveys (CSUR)* **41**(3), 1–58 (2009)
7. Chong, Y.S., Tay, Y.H.: Abnormal event detection in videos using spatiotemporal autoencoder. In: International Symposium on Neural Networks. pp. 189–196. Springer (2017)
8. Chowdhury, A., Dylov, D.V., Li, Q., MacDonald, M., Meyer, D.E., Marino, M., Santamaria-Pang, A.: Blood vessel characterization using virtual 3d models and convolutional neural networks in fluorescence microscopy. *IEEE ISBI 2017* pp. 629–632 (April 2017). <https://doi.org/10.1109/ISBI.2017.7950599>

9. Gatys, L.A., Ecker, A.S., Bethge, M.: Image style transfer using convolutional neural networks. In: *Proceedings of the IEEE Conference on Computer Vision and Pattern Recognition*. pp. 2414–2423 (2016)
10. Golan, I., El-Yaniv, R.: Deep anomaly detection using geometric transformations. In: *Advances in Neural Information Processing Systems*. pp. 9758–9769 (2018)
11. Gong, D., Liu, L., Le, V., Saha, B., Mansour, M.R., Venkatesh, S., Hengel, A.v.d.: Memorizing normality to detect anomaly: Memory-augmented deep autoencoder for unsupervised anomaly detection. In: *Proceedings of the IEEE International Conference on Computer Vision*. pp. 1705–1714 (2019)
12. Heljakka, A., Solin, A., Kannala, J.: Pioneer networks: Progressively growing generative autoencoder. In: *Asian Conference on Computer Vision*. pp. 22–38. Springer (2018)
13. Hinton, G.E., Salakhutdinov, R.R.: Reducing the dimensionality of data with neural networks. *science* **313**(5786), 504–507 (2006)
14. Huang, X., Liu, M.Y., Belongie, S., Kautz, J.: Multimodal unsupervised image-to-image translation. In: *Proceedings of the European Conference on Computer Vision (ECCV)*. pp. 172–189 (2018)
15. Johnson, J., Alahi, A., Fei-Fei, L.: Perceptual losses for real-time style transfer and super-resolution. In: *European conference on computer vision*. pp. 694–711. Springer (2016)
16. Karras, T., Aila, T., Laine, S., Lehtinen, J.: Progressive growing of gans for improved quality, stability, and variation. *arXiv preprint arXiv:1710.10196* (2017)
17. Kothari, S., Phan, J.H., Stokes, T.H., Wang, M.D.: Pathology imaging informatics for quantitative analysis of whole-slide images. *Journal of the American Medical Informatics Association: JAMIA* **20**(6), 10991108 (2013). <https://doi.org/10.1136/amiajnl-2012-001540>
18. Krizhevsky, A., Hinton, G.: Learning multiple layers of features from tiny images. *Tech. rep., Citeseer* (2009)
19. Netzer, Y., Wang, T., Coates, A., Bissacco, A., Wu, B., Ng, A.Y.: Reading digits in natural images with unsupervised feature learning (2011)
20. Nguyen, A., Yosinski, J., Clune, J.: Deep neural networks are easily fooled: High confidence predictions for unrecognizable images. In: *Proceedings of the IEEE conference on computer vision and pattern recognition*. pp. 427–436 (2015)
21. Ouardini, K., Yang, H., Unnikrishnan, B., Romain, M., Garcin, C., Zenati, H., Campbell, J.P., Chiang, M.F., Kalpathy-Cramer, J., Chandrasekhar, V., et al.: Towards practical unsupervised anomaly detection on retinal images. In: *Domain Adaptation and Representation Transfer and Medical Image Learning with Less Labels and Imperfect Data*, pp. 225–234. Springer (2019)
22. Perera, P., Nallapati, R., Xiang, B.: Ocgan: One-class novelty detection using gans with constrained latent representations. In: *Proceedings of the IEEE Conference on Computer Vision and Pattern Recognition*. pp. 2898–2906 (2019)
23. Ruff, L., Görnitz, N., Deecke, L., Siddiqui, S.A., Vandermeulen, R., Binder, A., Müller, E., Kloft, M.: Deep one-class classification. In: *International Conference on Machine Learning*. pp. 4390–4399 (2018)
24. Russakovsky, O., Deng, J., Su, H., Krause, J., Satheesh, S., Ma, S., Huang, Z., Karpathy, A., Khosla, A., Bernstein, M., et al.: Imagenet large scale visual recognition challenge. *International journal of computer vision* **115**(3), 211–252 (2015)
25. Schlegl, T., Seeböck, P., Waldstein, S.M., Schmidt-Erfurth, U., Langs, G.: Unsupervised anomaly detection with generative adversarial networks to guide marker discovery. In: *International Conference on Information Processing in Medical Imaging*. pp. 146–157. Springer (2017)

26. Tang, Y.X., Tang, Y.B., Han, M., Xiao, J., Summers, R.M.: Deep adversarial one-class learning for normal and abnormal chest radiograph classification. In: Medical Imaging 2019: Computer-Aided Diagnosis. vol. 10950, p. 1095018. International Society for Optics and Photonics (2019)
27. Tuluptceva, N., Bakker, B., Fedulova, I., Konushin, A.: Perceptual image anomaly detection. In: Palaiahnakote, S., Sanniti di Baja, G., Wang, L., Yan, W.Q. (eds.) Pattern Recognition. pp. 164–178. Springer International Publishing, Cham (2020)
28. Vahadane, A., Peng, T., Sethi, A., Albarqouni, S., Wang, L., Baust, M., Steiger, K., Schlitter, A.M., Esposito, I., Navab, N.: Structure-preserving color normalization and sparse stain separation for histological images. *IEEE transactions on medical imaging* **35**(8), 1962–1971 (2016)
29. Wang, X., Peng, Y., Lu, L., Lu, Z., Bagheri, M., Summers, R.M.: Chestx-ray8: Hospital-scale chest x-ray database and benchmarks on weakly-supervised classification and localization of common thorax diseases. In: Proceedings of the IEEE conference on computer vision and pattern recognition. pp. 2097–2106 (2017)
30. Zhai, S., Cheng, Y., Lu, W., Zhang, Z.: Deep structured energy based models for anomaly detection. *arXiv preprint arXiv:1605.07717* (2016)
31. Zhang, R., Isola, P., Efros, A.A., Shechtman, E., Wang, O.: The unreasonable effectiveness of deep features as a perceptual metric. In: Proceedings of the IEEE Conference on Computer Vision and Pattern Recognition. pp. 586–595 (2018)
32. Zhou, C., Paffenroth, R.C.: Anomaly detection with robust deep autoencoders. In: Proceedings of the 23rd ACM SIGKDD International Conference on Knowledge Discovery and Data Mining. pp. 665–674 (2017)

## Supplementary Material: Anomaly Detection with Deep Perceptual Autoencoders

Nina Tuluptceva<sup>1,2</sup>[0000-0003-0910-188X], Bart Bakker<sup>1</sup>[0000-0002-1438-8136],  
Irina Fedulova<sup>1</sup>[0000-0002-5959-5382], Heinrich Schulz<sup>1</sup>[0000-0003-4048-2254], and  
Dmitry V. Dylov<sup>2</sup>[0000-0003-2251-3221]

<sup>1</sup> Philips Research

nina.tuluptceva, bart.bakker@philips.com  
irina.fedulova, heinrich.schulz@philips.com

<sup>2</sup> Skolkovo Institute of Science and Technology  
d.dylov@skoltech.ru

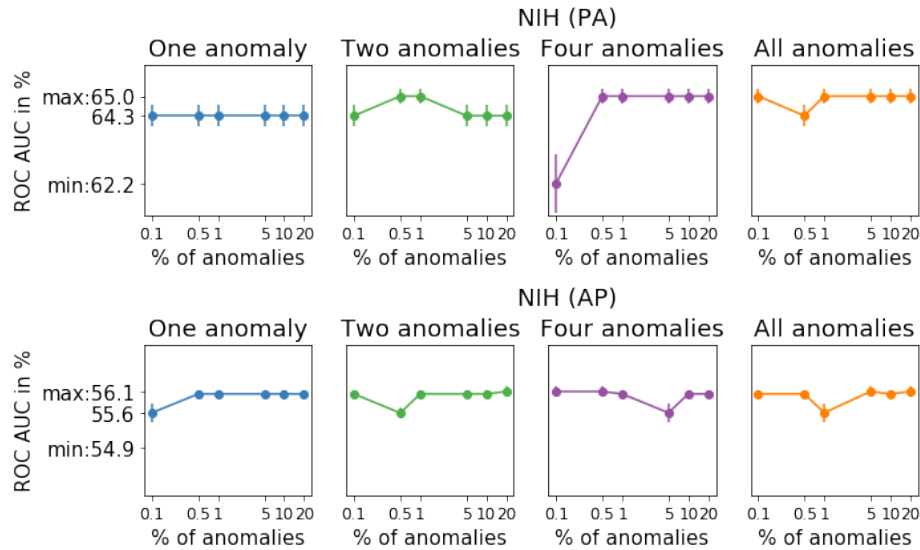


Fig. 1: Dependence of the quality of anomaly detection on the number of anomaly examples (the x-axis) and their variability (plot's title) in the validation set. This experiment shows that 0.5% of examples of one type of anomaly are enough to select optimal hyperparameters.

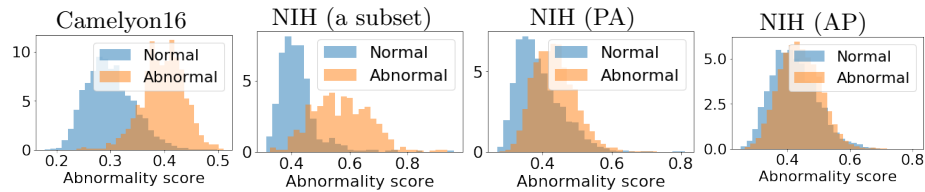


Fig. 2: Histograms of predicted abnormality scores for normal and abnormal images.

Table 1: Mean ROC AUC (in %, averaged over all classes) on natural images of CIFAR10 and SVHN datasets. Baseline results: authors’ default hyperparameters (left), cross-validated (right).

	AnoGAN	GANomaly	DSEBM	DeepSVDD	Deep GEO	PIAD	Deep IF	Ours
CIFAR10	57.6/-	58.1/-	64.8/-	58.8/-	86.6/86.5	78.8/81.3	87.2/ <b>87.3</b>	84.0
SVHN	53.3/-	-	57.3/-	57.1/-	93.3/ <b>93.5</b>	77.0/76.3	59.0/62.4	80.3

Table 2: ROC AUC in % with std on CIFAR 10 and SVHN per each class.

CIFAR10										
	plane	car	bird	cat	deer	dog	frog	horse	ship	truck
Deep GEO	75.7 $\pm 1.0$	96.0 $\pm 0.2$	<b>80.4</b> $\pm 1.1$	72.9 $\pm 0.9$	88.0 $\pm 0.2$	<b>86.3</b> $\pm 0.9$	84.6 $\pm 0.5$	<b>95.4</b> $\pm 0.0$	<b>94.3</b> $\pm 0.2$	91.4 $\pm 0.5$
PIAD	84.3 $\pm 0.2$	86.7 $\pm 1.1$	74.4 $\pm 0.9$	59.6 $\pm 2.1$	85.0 $\pm 1.1$	73.6 $\pm 1.1$	83.8 $\pm 1.2$	87.0 $\pm 1.1$	88.8 $\pm 0.2$	89.4 $\pm 0.7$
Deep IF	<b>87.1</b> $\pm 0.9$	<b>97.0</b> $\pm 0.3$	75.2 $\pm 2.9$	<b>73.7</b> $\pm 1.8$	<b>88.9</b> $\pm 1.0$	85.0 $\pm 2.6$	<b>90.5</b> $\pm 0.9$	86.3 $\pm 1.7$	93.4 $\pm 0.3$	<b>95.7</b> $\pm 0.3$
<b>Ours</b>	86.5 $\pm 0.2$	92.2 $\pm 0.3$	76.8 $\pm 0.6$	59.4 $\pm 0.0$	85.7 $\pm 0.1$	77.7 $\pm 0.9$	88.8 $\pm 0.3$	89.5 $\pm 0.8$	91.4 $\pm 0.5$	92.2 $\pm 0.4$
SVHN										
	0	1	2	3	4	5	6	7	8	9
Deep GEO	<b>90.6</b> $\pm 0.6$	<b>84.8</b> $\pm 0.6$	<b>97.2</b> $\pm 0.2$	<b>91.1</b> $\pm 0.1$	<b>97.5</b> $\pm 0.1$	<b>96.3</b> $\pm 0.0$	<b>96.2</b> $\pm 0.2$	<b>98.4</b> $\pm 0.0$	<b>85.6</b> $\pm 0.9$	<b>97.6</b> $\pm 0.2$
PIAD	86.3 $\pm 0.9$	80.2 $\pm 0.9$	76.2 $\pm 0.8$	71.4 $\pm 1.1$	77.0 $\pm 0.5$	71.9 $\pm 0.9$	70.6 $\pm 0.5$	78.4 $\pm 0.2$	79.6 $\pm 0.7$	71.9 $\pm 0.8$
Deep IF	75.0 $\pm 1.2$	70.5 $\pm 1.5$	51.1 $\pm 0.8$	59.0 $\pm 0.9$	57.7 $\pm 1.4$	68.4 $\pm 0.6$	54.5 $\pm 0.2$	58.7 $\pm 0.7$	69.6 $\pm 1.6$	59.1 $\pm 1.5$
<b>Ours</b>	88.4 $\pm 0.2$	82.7 $\pm 0.8$	80.0 $\pm 0.8$	72.9 $\pm 0.1$	78.7 $\pm 0.7$	77.4 $\pm 0.7$	78.0 $\pm 0.8$	79.0 $\pm 0.2$	83.5 $\pm 0.2$	82.1 $\pm 0.3$